doi:10.1016/j.jmb.2006.03.064 J. Mol. Biol. (2006) 359, 1107–1124

JMB

Available online at www.sciencedirect.com

SCIENCE DIRECT®

ELSEVIER

Regulatory Dynamics of Synthetic Gene Networks with Positive Feedback

Yusuke T. Maeda* and Masaki Sano

Department of Physics, Graduate School of Science TheUniversity of Tokyo, 7-3-1 Hongo, Bunkyo-ku, Tokyo 113-0033, Japan

*Corresponding author

Biological processes are governed by complex networks ranging from gene regulation to signal transduction. Positive feedback is a key element in such networks. The regulation enables cells to adopt multiple internal expression states in response to a single external input signal. However, past works lacked a dynamical aspect of this system.

To address the dynamical property of the positive feedback system, we employ synthetic gene circuits in *Escherichia coli* to measure the rise-time of both the no-feedback system and the positive feedback system. We show that the kinetics of gene expression is slowed down if the gene regulatory system includes positive feedback. We also report that the transition of gene switching behaviors from the hysteretic one to the graded one occurs. A mathematical model based on the chemical reactions shows that the response delay is an inherited property of the positive feedback system. Furthermore, with the aid of the phase diagram, we demonstrate the decline of the feedback activation causes the transition of switching behaviors. Our findings provide a further understanding of a positive feedback system in a living cell from a dynamical point of view.

Keywords: systems biology; synthetic biology; positive feedback; dynamics; hysteresis

Introduction

One of the central focuses in post-genomic research is to understand how biological phenomena arise from the interactions between genes and proteins. These interactions are incorporated into complex regulatory networks. Recently, the potential reduction of these systems to smaller functional motifs has been proposed. To make progress toward understanding how sets of regulatory motifs interact in a large-scale network, several studies have characterized the properties of elemental regulatory systems, e.g. feed-forward loops[1,2] and feedback systems.[3–5] It is of interest to study the property of the regulatory structure in the biological network.

One of the ubiquitous regulatory systems is a feedback system. This system uses its output as a regulatory input to perform a number of functions. One type of feedback is negative feedback, in which transcription factors negatively regulate their own transcription. A single-step negative feedback reduces cell-to-cell fluctuations in the steady state of transcription factors,[3] alters the spectra of gene expression noise[6] and speeds up the dynamics of gene expression.[7] A double negative feedback system in which each of two regulatory factors negatively regulates the synthesis of the other toggles the gene switch and exhibits hysteresis in the steady state.[8,9] These properties play a central role on diverse processes, e.g. differentiation.[10]

Another important feedback system is the positive feedback system (PFS). Theoretical and experimental works have found that cells with the PFS exhibit a bistable response, switching between discrete stable steady states without being able to rest in intermediate states.[4,11,12] This implies that a single-gene switch can be constructed as an alternative to double negative feedbacks. Such a PFS is included in the bacteriophage lambda lytic-lysogeny switch,[13] nutrients utilization systems,[14–16] several signaling cascades[17–19] and cell cycle regulatory circuits.[20,21]

However, bistability is not a sole property of the PFS. Savageau has predicted that positive feedback

Abbreviations used: PFS, positive feedback system; NFS, no feedback system; IPTG, isopropyl thio β-D-galactosidase; wt, wild-type; GFP, green fluorescent protein.

E-mail address of the corresponding author: y-maeda@daisy.phys.s.u-tokyo.ac.jp

slows down the kinetics of protein synthesis.[22] Although past works have not focused on a dynamical aspect of positive feedback, it is important to know how cells reach to the steady state.

Here, we explore properties of the dynamical behavior of gene expression by focusing on the rise-time; which is defined as the time required for the gene product to reach half of its steady-state concentration. We synthesize three positive feedback systems in *Escherichia coli* by using the elements from the lambda phage lysogenic system.[23] Employing a relatively simple genetic circuit out of well-characterized elements that do not comparatively interfere with intrinsic components avoids the impairing cell viability. Comparing difference between the no-feedback system (NFS) and the PFS, we show that the kinetics of the PFS is slower than that of the NFS. We also show that two of three PFSs exhibit the hysteretic gene expression but one of them does the graded one. Next, we propose the mathematical model to answer the following questions. (I) What mechanism generates the response delay? (II) What mechanisms convert the hysteretic gene expression to the graded one? (III) Is there an inevitable relation between the response delay and hysteresis? The analysis of a mathematical model together with experimental data reveals that the response delay of the PFS results from the accumulation of activator proteins. Furthermore, with the aid of the phase diagram, we find that the rate of the feedback activation transits the switching behaviors. Finally, we discuss the biological function of response delay and hysteresis. These results may help in further understanding of biological phenomena involving the PFS especially from a dynamical viewpoint.

Results

Design of the synthetic genetic networks

To explore a dynamical property of the positive feedback system (PFS), we employed the artificial genetic network system. The PFS was isolated from the promoter P_{RM} and the *cI* gene of bacteriophage lambda. These genetic elements provide positive feedback as follows. The P_{RM} promoter transcribes *cI* in a lysogen.[13,24] This promoter consists of three tandem operational sites, OR1, OR2 and OR3. These OR sites also play a role as the another promoter: the lytic promoter P_R, from which RNA polymerase transcribes *cro* and several early lytic genes. Two kinds of repressor dimers, CI and Cro can bind to these OR sites. The binding affinities for CI of these sites are such that at increased concentrations CI initially binds to OR1, then OR2 and finally OR3. The binding affinities for Cro are such that it will first bind to OR3 and then to OR1 and OR2. It is the occupancy of these sites that determines which one of the two promoters that are active. CI monomers dimerize and then CI dimer binds tightly to OR1. The binding of CI dimer to OR1 prevents the binding of the RNA polymerase to the P_R promoter and thus causes a further repression of transcription of *cro* from the P_R promoter. When bound to the OR2 site, the CI protein can interact with the σ-factor in the RNA polymerase holoenzyme and increase the rate of transcription from P_{RM}. Hence, CI positively regulates its own synthesis and its feedback activation will ensure that sufficiently high levels of CI protein are presented to maintain the phage in the lysogenic state. When the concentration of CI proteins is high, the CI dimer binds to the low-affinity OR3 site and represses the transcription of its own gene. The OR3 occupation ensures that the rate of transcription of the *cI* gene is never high to respond to endogenous signals produced by the host cell.

To synthesize the PFS, we positioned the P_{RM} promoter upstream of the *cI-gfp*(*aav*) fusion gene (Figure 1(a)). Although the P_{RM} promoter is intrinsically the weak promoter, the binding of CI-GFP(AAV) dimer to OR1, OR2 enhances the promoter activity.[25] This molecular mechanism can make CI dimers positively regulate its own synthesis. We call such a regulation the feedback activation. Then, P_{RM} transcribes *cI-gfp*(*aav*) by CI-GFP(AAV) dependent manner. For the tuning of the transcription initiation, the P_{RM} promoter was modified to include the lactose operator *lacO* downstream of the promoter.[26] In this study, we adopted the O1 type of *lacO*. A chromosomally expressing lactose repressor protein LacI, binds to the lactose operator and inhibits gene expression from the upstream promoter because LacI excludes RNA polymerase from DNA strand. The chemical inducer IPTG inactivates LacI. By varying the IPTG concentration, one can tune the transcription of the downstream gene by removing the LacI. Therefore, the P_{RM} promoter activity is fully repressed in the absence of IPTG. Hereinafter we call this regulatory system the P_{RM} wild-type positive feedback system (P_{RM} wt-PFS).

As a control, we constructed the $P_{trc\text{-}2}$::*gfp*(*aav*) as a no-feedback system (NFS) (Figure 1(b)). No-feedback means the absence of feedback regulation by activator proteins while other molecular processes, a maximal promoter activity and protein degradation, are identical with those of the PFS. The transcription from $P_{trc\text{-}2}$ can be controlled by IPTG because this promoter includes the *lacO* operator, the same as P_{RM}-*lacO*.

In addition, we constructed the mutated P_{RM} promoter: P_{RM}L1L1R3 and P_{RM}R3R2R3 (Figure 1(c) and (d)). Further, we integrated *lacO* downstream of these promoters as same as P_{RM}-*lacO*. The former promoter P_{RM}L1L1R3, which was constructed by replacing each of OR1 and OR2 with the OL1 site contained three adjacent sites OL1(upstream), OL1(downstream), OR3. The OL1 operator is one of the operator sites in the P_L promoter that can be bound by the CI protein. The binding affinity of CI to OL1 is larger than that of each of OR1 and OR2.[27] According to the *in vitro* studies, on both OR and OL, we assume that CI dimers initially bind to

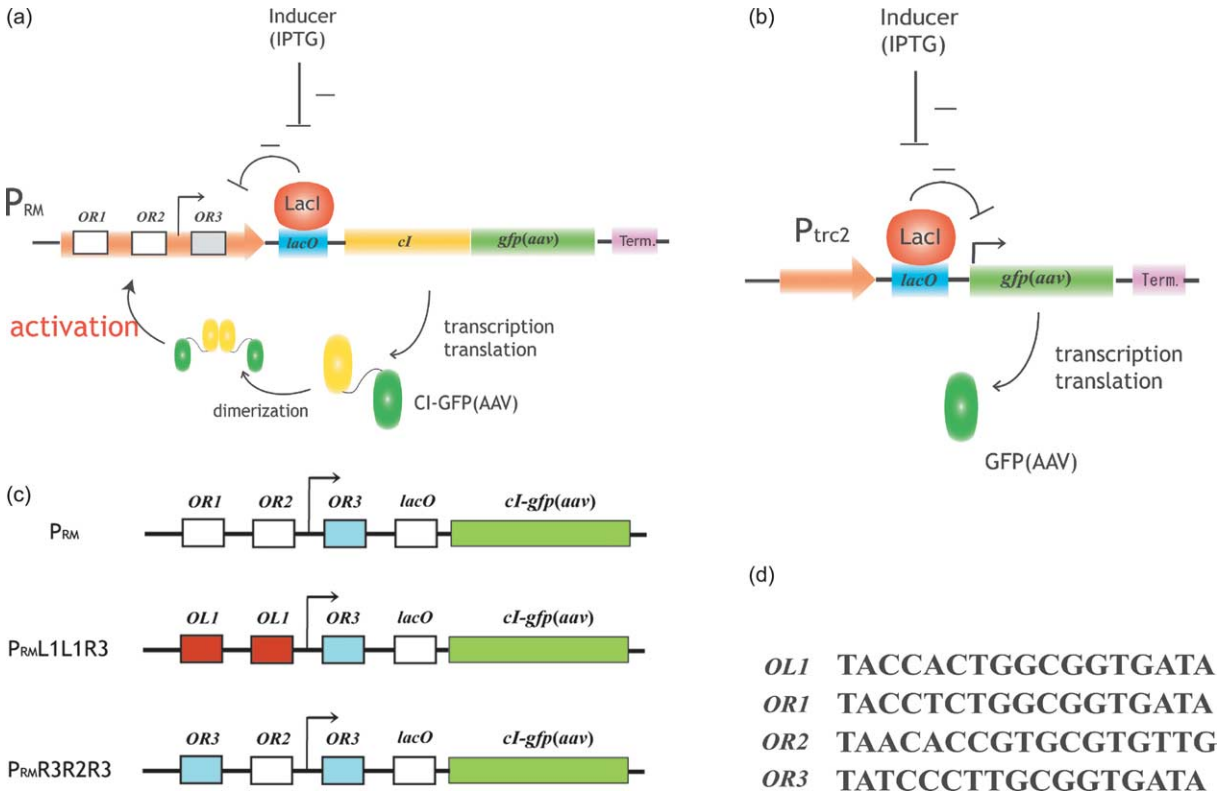

Figure 1. Design of the gene expression systems. (a) The P_{RM} wild-type positive feedback system. The promoter region contains three operator sites, known as OR1–OR3. The *cI-gfp*(AAV) gene encodes the activator protein. CI-GFP(AAV) dimerizes and binds to one of the three binding sites, OR1, OR2 (activation) or OR3 (repression). We fused the lactose operator, *lacO*, downstream of the P_{RM} promoter. A chromosomally encoded lactose repressor, LacI, binds to *lacO* and represses the transcription of the *cI-gfp*(AAV) gene. The inducer IPTG binds and inactivates LacI, causing the expression of CI-GFP(AAV). (b) The no-feedback system. This system has a P_{trc-2} promoter instead of P_{RM}-*lacO*. Cells expressing GFP can be induced by IPTG, just as in the positive feedback system except for the lacking *cI* region. (c) Variants of the P_{RM} promoter. The λ-phage P_{RM} promoter contains three neighboring binding sites: OL1, OR1 and OR2. They allow cooperative activation. (d) The OL1, OR1, OR2, OR3 sequence.

whether the upstream OL1 or the downstream one alternatively, then the remaining OL1 and finally OR3 as the CI concentration increases. We call the PFS with P_{RM}L1L1R3-*lacO* as the P_{RM}L1L1R3 positive feedback system (P_{RM}L1L1R3-PFS). The latter promoter P_{RM}R3R2R3 was constructed by substituting OR1 with OR3. The order of a CI dimer binding to these sites are such that dimers firstly bind to OR2, then whether the upstream OR3 or alternative downstream one, and finally another OR3.[28] We also call the PFS with P_{RM}R3R2R3-*lacO* as the P_{RM}R3R2R3 positive feedback system (P_{RM}-R3R2R3-PFS).

The dynamics of positive feedback: positive feedback shows response-delay

To study the response kinetics of the PFS, the time-evolution of gene expression from cultures bearing the reporter plasmid was measured by the automated multiwell fluorimeter.[7] Green fluorescent protein (GFP) fluorescence and optical absorbance A_{600} were measured at about 5 min intervals. Cultures were maintained within the mid-exponential growth phase during the measurements. Gene expression was induced by adding IPTG. The raw time dependence of the fluorescence intensity was smoothened with a window size of four activities. We define the rise-time τ, as that required for a gene-expressed product to reach half of its steady-state concentration, $x(\tau)=x_{max}/2$. The observed GFP fluorescence reflects the total CI-GFP(AAV) fluorescence including CI-GFP(AAV) monomers, free dimers and DNA–dimer complexes.

The GFP fluorescence from cells with the P_{RM} wt-PFS increases slower than that with the NFS (Figure 2(a)). After the short time lag, the fluorescence of the NFS is rapidly expressed and then the promoter activity saturated to the constant (Figure 2(a), blue). The rise-time of the NFS is 50 min ($\tau_{NFS}=50$ min). The kinetics differ significantly from that of the P_{RM} wt-PFS. In the PFS, the increment in the promoter activity of the P_{RM} wt-PFS is small for the low CI-GFP(AAV) range (Figure 2(a), red). However, at a later time (after 50 min) when the activator concentration is in an intermediate range, a small increase in the activator concentration results in a large change of the production rate. The rise-time of the P_{RM}wt-PFS is

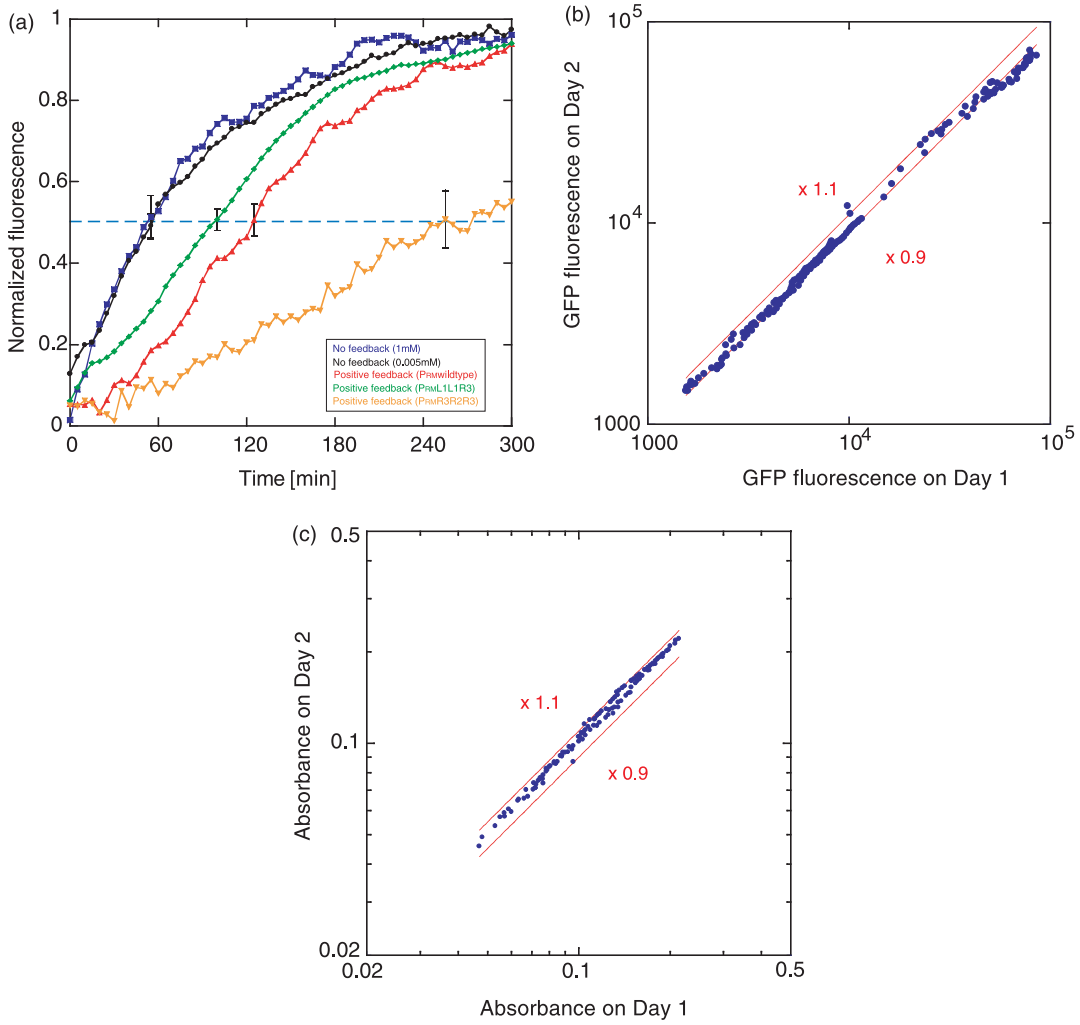

Figure 2. (a) Experimental dynamical behaviors of the synthetic genetic networks. Fluorescence per one cell, normalized by its maximal value, is plotted *versus* time. The rise-time is the time taken to reach half of the maximal product concentration. This is the time at which the curves intersect the horizontal line at relative fluorescence = 0.5. Blue, the NFS (IPTG = 1 mM); black, the NFS (IPTG = 0.005 mM); red, the P_{RM}wt-PFS; green, the P_{RM}L1L1R3-PFS; orange, the P_{RM}R3R2R3-PFS. Maximal fluorescence of the NFS (IPTG = 0.005 mM) is comparable in intensity to that of the P_{RM}wt-PFS. The error bars are standard deviation at rise-time. (b) and (c) Day-to-day reproducibility of the high-resolution measurement. Unaveraged GFP fluorescence (b) and absorbance (c) (background subtracted) for repeated experiments performed on different days. The mean relative errors for the absorbance and fluorescence measurements are 10%, respectively.

120 min ($\tau_{wtPFS} = 120$ min), which corresponds to approximately one and one third of a cell cycle. To evaluate the response delay, we define $\tau - \tau_{NFS}$ as the delay time. The delay time of the P_{RM}wt-PFS is 70 min, which is approximately 0.8 times of a cell cycle. However, comparing the two systems at 1 mM IPTG, the maximal fluorescence of the NFS is ten times as large as that of the P_{RM}wt-PFS. In order to exclude the possibility that the response delay arises from the difference of the promoter activity, we measured the time-evolution of the NFS at 0.005 mM IPTG. The maximal GFP expression of the NFS at 0.005 mM IPTG is approximately comparable to that of the P_{RM}wt-PFS at 1 mM IPTG. We find that the dynamics do not depend on the maximal level of protein (Figure 2(a), black and blue). This result suggests that the response delay is independent of the maximal saturation level of the gene product. Then, we note that the fusion construct of the P_{RM}wt-PFS is identical with the bi-cistronic one at the dynamics level (see Supplementary Data, Figure S1). We conclude that the response delay is an intrinsic property of the PFS.

For the further characterization of the dynamical property of the positive feedback system, we examine whether the rise-time is increased or decreased by genetic mutations. As seen in Figure 2(a) (green), the rise-time of the P_{RM}-L1L1R3-PFS at 1 mM IPTG is 90 min ($\tau_{L1L1R3\text{-}PFS} =$ 90 min), which corresponds to one cell cycle. The delay time is 40 min, which is approximately one half of a cell cycle. The P_{RM}L1L1R3-PFS exhibits the steeper, and its maximal fluorescence is 1.1-fold of the P_{RM}wt-PFS.

We constructed another mutated PFS: the P_{RM}-R3R2R3-PFS whose binding affinity of the CI dimer

to the uppermost-stream operator site becomes lower *in vitro*.[28] In contrast to the others, the P_{RM}R3R2R3-PFS at 1 mM IPTG shows the slowest kinetics. Its rise-time is 250 min ($\tau_{R3R2R3\text{-}PFS} =$ 250 min), which corresponds to 2.8 times a cell cycle. The delay time is 200 min, which is 2.2 times a cell cycle. Further, its maximal fluorescence is 0.7-fold of the P_{RM}wt-PFS.

These results suggest that (i) the rise-time of the PFS is larger than that of the NFS and (ii) the rise-time is influenced with the genetic mutation.

Positive feedback switches gene expression in a hysteretic or a graded manner

Another important characteristic of a PFS is its own history dependent behavior, so-called hysteresis. In other words, it is easier to maintain the system in its on state than to toggle it on and off. The system requires a larger signal to switch from low to high (low→high) comparing with from high to low (high→low); low means the state with the lower activator concentration, while high is the state with the higher activator concentration. However, cells with the PFS do not always exhibit hysteresis. Cells also switch gene expression in a graded manner. If a PFS expresses a gene gradually, the expression level moves reversibly between low and high. To determine whether the P_{RM} PFSs exhibit the hysteretic gene expression or the graded one, we performed the following experiment. The overnight cultures were grown in a fresh minimal medium with either the presence or absence of 1 mM IPTG. It is crucial to use cells with well-defined initial states, either high (at 1 mM IPTG) or low (at 0 mM IPTG), because the response of a hysteretic system is expected to depend on its history. Cells were maintained in a mid-exponential growth phase. GFP fluorescence was measured after six to seven generations. We determined whether they were hysteretic or not if the difference of CI-GFP(AAV) fluorescence between high→low and low→high was larger or smaller than the error values, respectively.

We find that cells with the P_{RM}wt-PFS expressed in a critically different manner between increasing (low→high) and decreasing (high→low) IPTG (Figure 3(a)). Cells that have been initially in the high CI-GFP(AAV) state remain in that state at IPTG concentrations >0.0025 mM. On the other hand, cells in the low state switch to the high state when treated with IPTG at 0.05 mM or higher. The hysteretic response is observed at IPTG concentrations of between 0.0025 mM and 0.05 mM. On the contrary, cells with the NFS exhibits not such a hysteresis but the graded response (Figure 3(b)).

Next, to determine whether cells with the variant PFS exhibit hysteresis or not, both the P_{RM}L1L1R3-PFS and P_{RM}R3R2R3-PFS were subjected to the same procedure. In P_{RM}L1L1R3-PFS, the hysteretic gene expression is observed at IPTG concentrations of between 0.005 mM and 0.02 mM (Figure 3(c)). However, the profile of P_{RM}R3R2R3-PFS is graded and reversible without showing any signs suggestive of hysteresis (Figure 3(d)). These results confirm that cells with the P_{RM} PFSs produce whether the hysteretic or the graded response.

We mention that *E. coli* has an inner PFS during lactose utilization. In this study, both the synthetic PFS and NFS can ignore the inner system. It is because glucose is included in the minimal medium and inhibits LacY protein.[12,29] Furthermore, glucose decreases the intracellular concentration of cAMP. Then, the transcriptional activator complex CRP–cAMP cannot induce the lac operon. Therefore, we can control gene expression without the concomitant maintenance. Thus, we consider that the positive feedback system could be controlled by the single parameter; the concentration of IPTG, I.

As shown, both the response delay and hysteresis are the major characteristics of the synthetic positive feedback systems. However, the following questions arise. (I) What mechanism generates the response delay? (II) What mechanism converts the response from hysteretic to the graded one? (III) Is there any inevitable relation between the response delay and hysteresis? To answer these questions, we present mathematical analyses based on the dynamics of gene expression in the following sections.

Mathematical analysis: the model and dynamics

First, to answer the question (I), we analyze the mathematical model describing the processes depicted in Figure 1. The model is the variant of the Collins model, which is derived from an application of the slow chemical reactions.[12] The main difference is that we ignore the influence of cell growth on chemical reactions. In Supplementary Data, we provide a detailed description of the derivation of the dynamical model. Although statistical mechanics models have been already proposed,[30,31] the present model is not meant to be a detailed account of the full biochemistry of the system, rather a simple model that captures the essential behavior.

For the NFS with the constant production rate, one assumes that:

$$\frac{dx}{dt} = \alpha(I) - \gamma x, \tag{1}$$

where x is the mean GFP concentration per one cell. The degradation term is defined as $-\gamma x$. The production term $\alpha(I)$ is the function of the IPTG concentrations, I. By simple mathematics, we obtain the rise-time of the NFS as $\tau = \ln 2/\gamma$. The effective degradation rate of protein is dependent on both proteolysis and cell division. However, the rise-time of the NFS (50 min) is larger than the expected value from the simple mathematics, 36 min (see Supplementary Data). The difference might be caused from (i) the initial lag-time in the gene expression, e.g. GFP maturation and transcription, or (ii) the over-simplification of mathematics. In this study, because

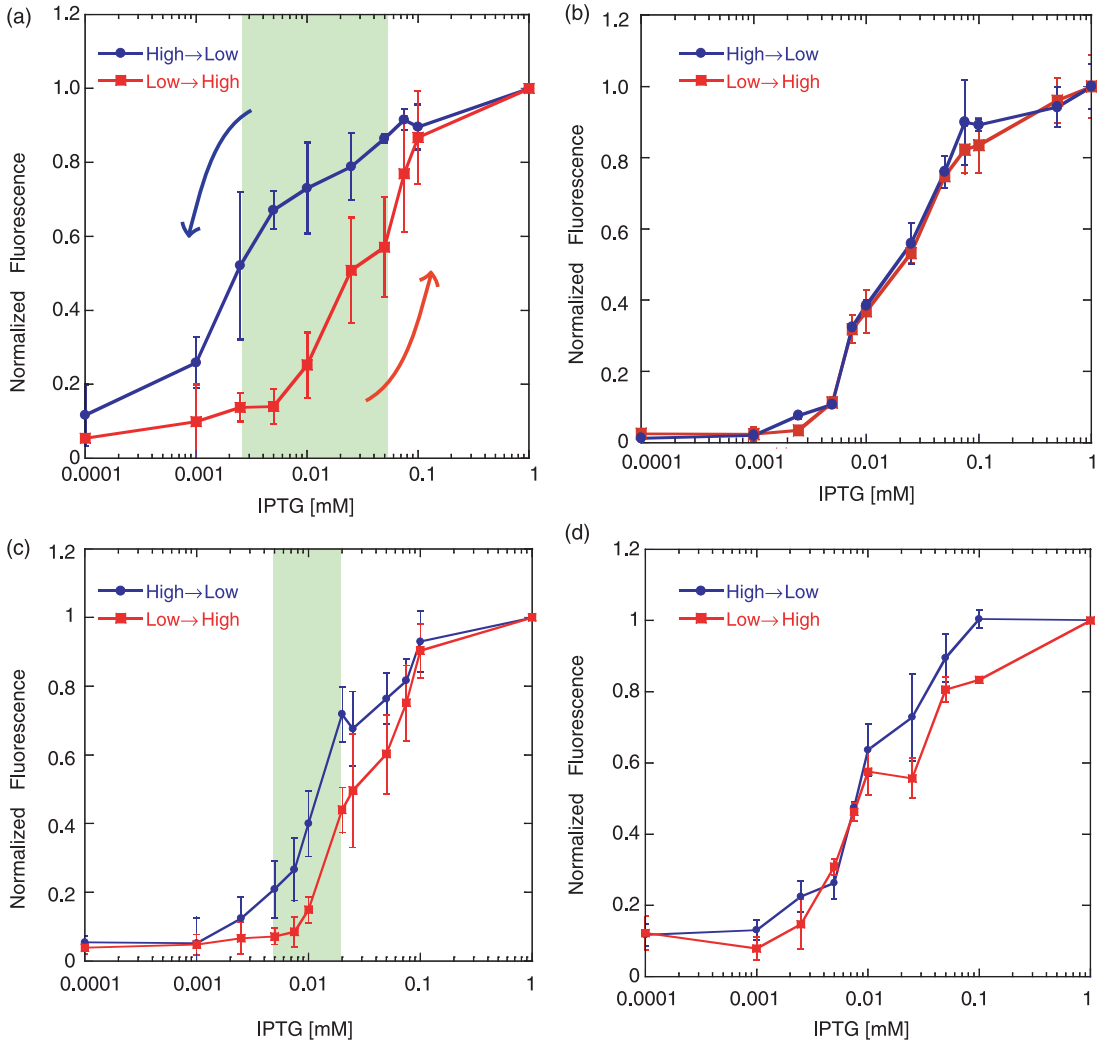

Figure 3. Hysteretic response or graded one in the positive feedback system. The mean GFP expression of (a) the P_{RM}wt-PFS, (b) the NFS, (c) the P_{RM}L1L1R3-PFS and (d) the P_{RM}R3R2R3-PFS *versus* the IPTG concentration of three independent experiments. Red, low→high (going up); blue, high→low (coming down). The green region shows the range of IPTG concentrations over which the gene expression occurs hysteretically. Cells in the high or low state were suspended and washed in a medium lacking IPTG, when diluted 1/100 into a medium containing the indicated IPTG concentration. Six to seven generations were grown, after which GFP fluorescence was measured.

our main focus is the dynamic property of the PFS, we do not try to pursue this inconsistency. In the meantime, we define the effective half-life of GFP as 50 min. It leads to $\gamma = 0.014$ (1/min).

The promoters used in the experiment are regulated by the lac operator system. According to the simple model for the lac regulated promoter,[32] the production term is defined as:

$$\alpha(I) = \alpha_{\max}\frac{s_I + I^2}{K_I + I^2}, \qquad (2)$$

where s_I is the basal rate of synthesis under the full repression, and K_I is the Michaelis constant of anti-repression. This function represents the promoter activity, which is regulated by IPTG. $\alpha_{\max}$ is the maximal rate of production from promoter.

The simulated result agrees well with experiments in the case with the NFS (Figure 4(a), blue).

A PFS is one in which the production rate depends on the intracellular concentration of the gene product. The following model is derived from a straightforward application of the chemical kinetics describing the processes depicted in Figure 1(a). The time evolution of the number of CI-GFP(AAV) monomers is:

$$\frac{dx}{dt} = \frac{1}{h(x)}(f(x,I) - \gamma x), \qquad (3)$$

where x is the mean concentration of the CI-GFP(AAV) monomer per one cell. The production term $f(x,I)$ represents the effect of the transcription and translation, whereas $h(x)$ arises from the vast separation of time scales set by the transcription and protein dimerization rates. This model is closely similar to the Collins model.[12] Their

functional forms are as follows:

$$f(x,I) = \alpha(I)\frac{1 + K_1K_2x^2 + \beta K_1K_2K_3x^4}{1 + K_1K_2x^2 + K_1K_2K_3x^4 + K_1K_2K_3K_4x^6} \tag{4}$$

$$h(x) = 1 + 4K_1x + 4K_1K_2xO_0(x) + 16K_1K_2K_3x^3O_0(x) + 36K_1K_2K_3K_4x^5O_0(x), \tag{5}$$

$$O_0(x) = \frac{m}{1 + K_1K_2x^2 + K_1K_2K_3x^4 + K_1K_2K_3K_4x^6}, \tag{6}$$

$$X = x + 2K_1x^2 + 2K_1K_2x^2O_0(x) + 4K_1K_2K_3x^4O_0(x) + 6K_1K_2K_3K_4x^6O_0(x), \tag{7}$$

where X is the total concentration of CI-GFP(AAV) per one cell, and $O_0(x)$ represents the promoter concentration with no CI dimer. The form of the production term $f(x,I)$ dictates the equilibrium number of CI monomers. The even polynomials in x occur due to the dimerization and the subsequent binding to the operator sites. We ignore cooperative non-specific DNA binding by octamerizing CI proteins because the differences between non-specific and specific binding affinities for CI repressor are large.[33] K_1 represents the dimerization affinity of CI monomers. K_i (i=2–4) represents the

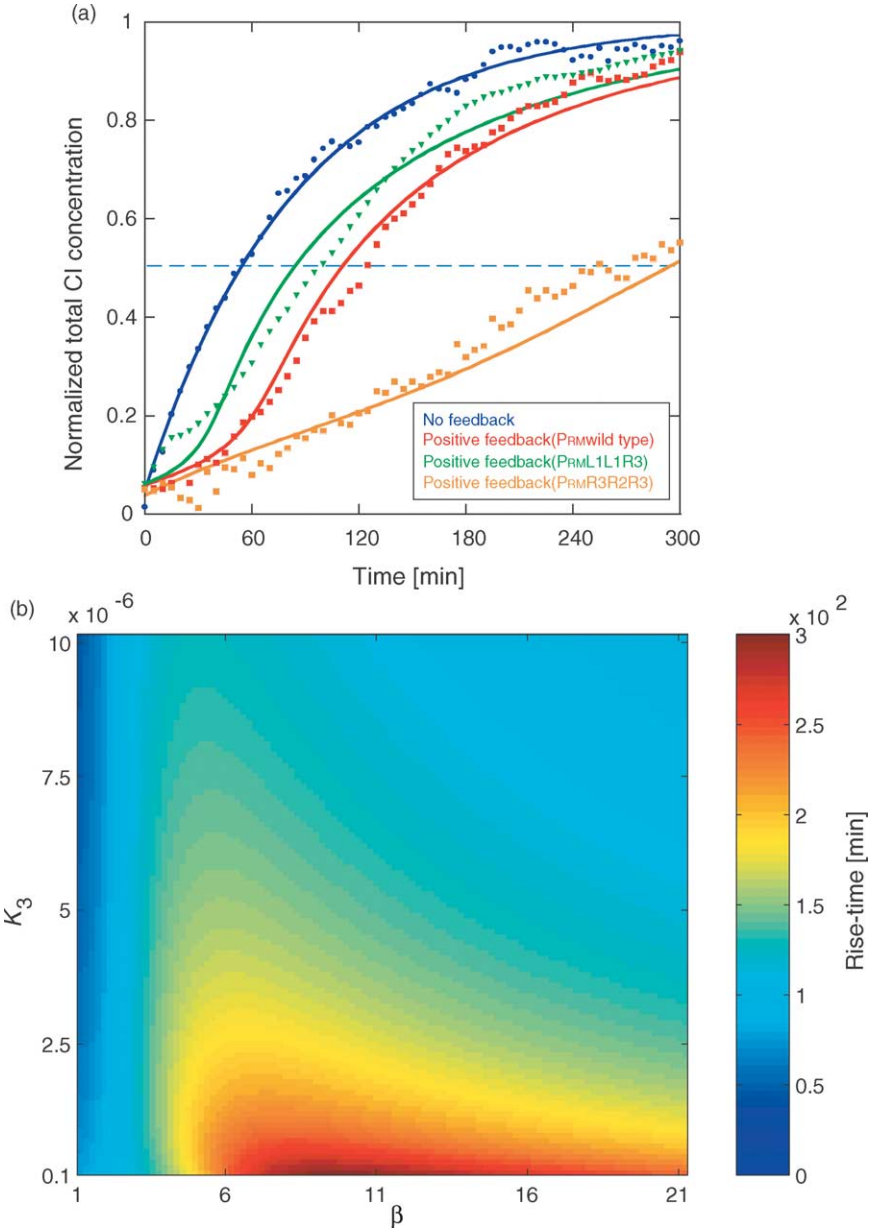

Figure 4 (*legend on page 1116*)

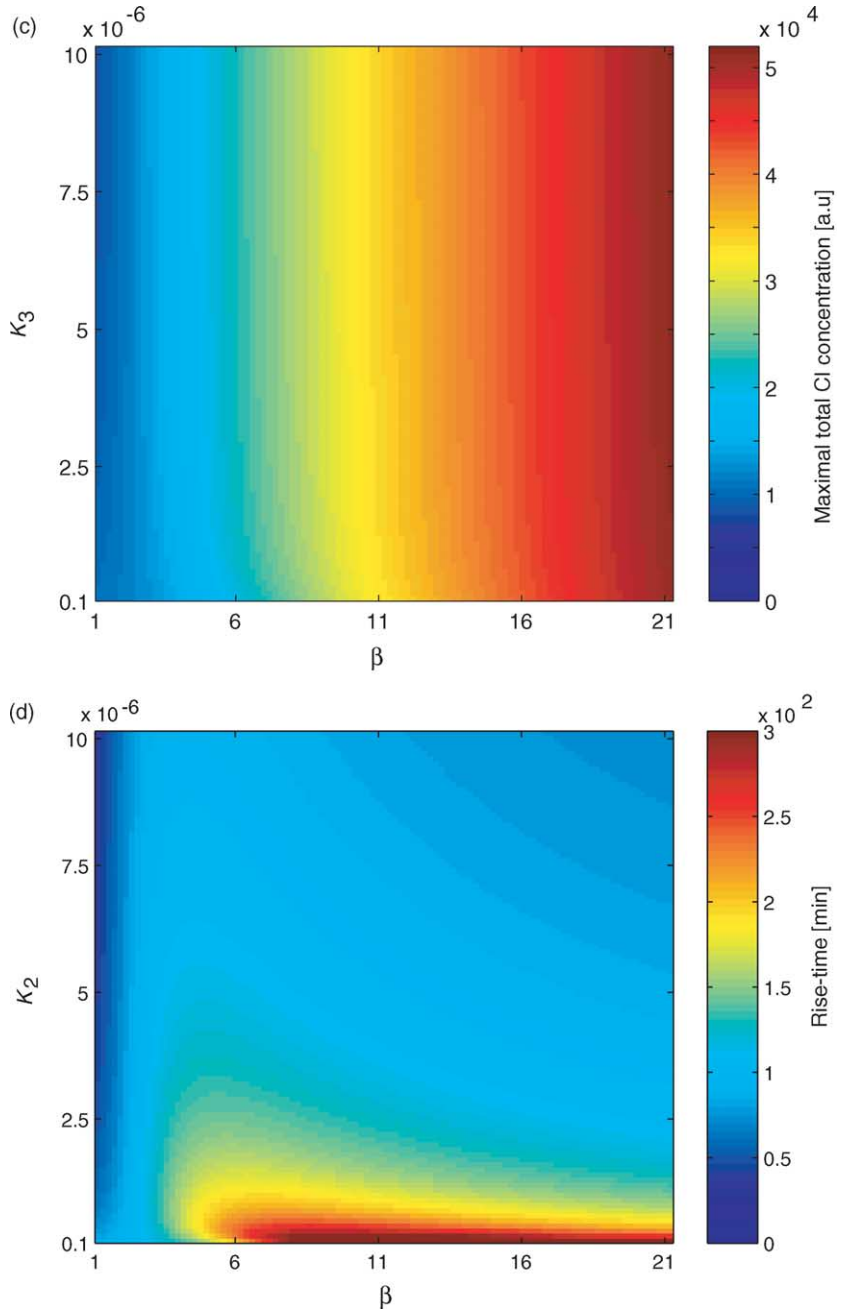

Figure 4 (*legend on page 1116*)

binding affinity of the activator to operator sites. β denotes the ratio of the transcriptional activity of the two CI dimers binding state to the no activator binding state. K_i/K_2 (i=3,4) denotes the relative affinities for dimer binding to OR1 *versus* that of binding to OR2 or OR3. The fact that $\beta > 1$ on the x^4 term is present because transcription is enhanced when the two operator sites OR1 and OR2 are occupied. The x^6 term represents the occupation of all three operator sites and disappears from the numerator, because the OR3 occupation by the CI dimer inhibits polymerase binding and shuts off transcription. Because only CI can activate transcription, the promoter activity increases with the CI concentration. Utilizing equation (2), we can rewrite the production function as:

$$f(x,I) = \alpha_{\max} \frac{s_I + I^2}{K_I + I^2} \times \frac{1 + K_1K_2x^2 + \beta K_1K_2K_3x^4}{1 + K_1K_2x^2 + K_1K_2K_3x^4 + K_1K_2K_3K_4x^6}, \quad (8)$$

where $\alpha_{\max}$ is the maximal rate of synthesis.

Then, we performed the best-fit random parameterization (see Materials and Methods) with the reference to the molecular biological research. The theoretical kinetics of each of the systems reproduces the experiment well (Figure 4(a)). The

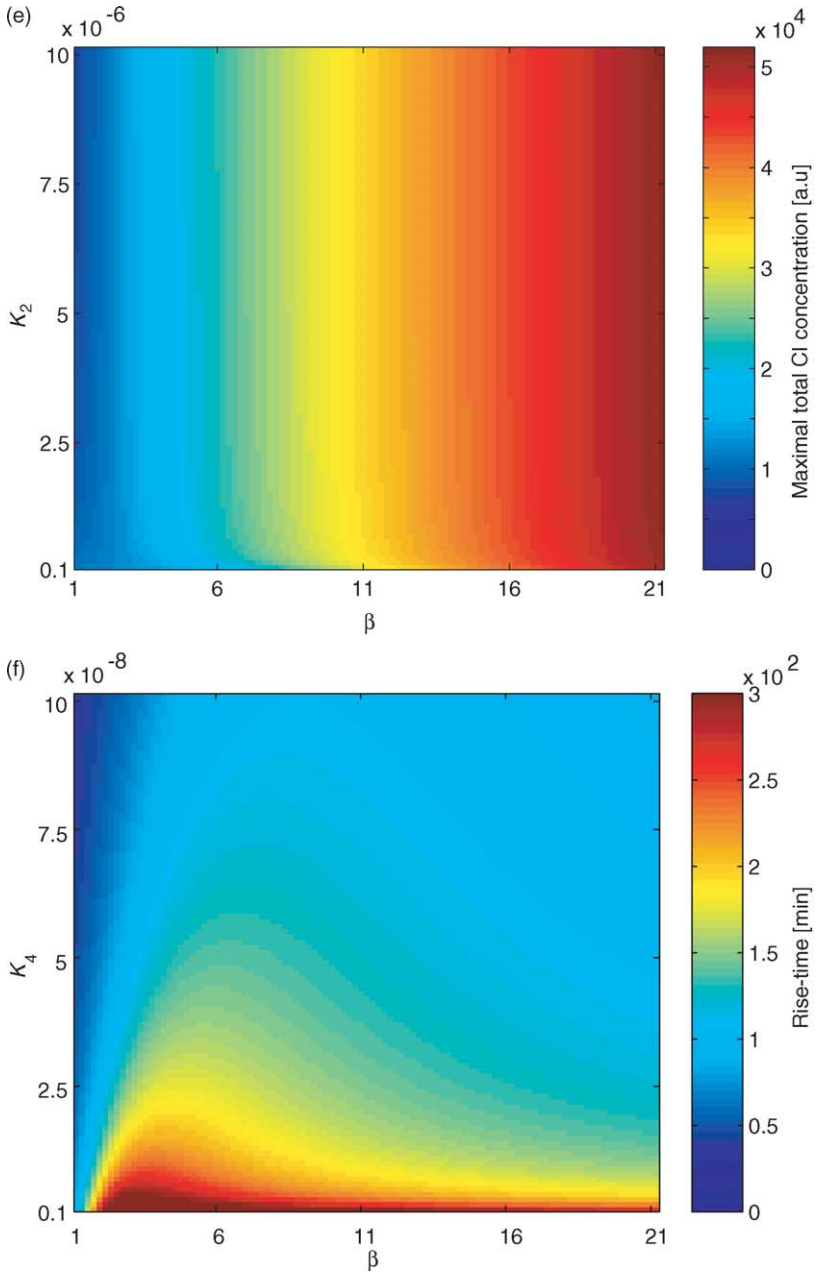

Figure 4 (*legend next page*)

parameters appearing in equations are listed in Table 1.

For the operator region, we obtain $K_3/K_2 \approx 5$, $K_4/K_2 \approx 0.03$, $\beta \approx 18$ in P_{RM}wt-PFS. In the P_{RM}L1L1R3-PFS, the expected increase of both K_2 and K_3 are observed. In the P_{RM}L1L1R3-PFS, the ratios of the CI binding affinities are $K_3/K_2 \approx 4$ and $K_4/K_2 \approx 0.02$. Further, $\beta \approx 21$ is larger than that of the P_{RM}wt-PFS. In the P_{RM}R3R2R3-PFS, parameters β and K_4 are smaller than those of the P_{RM}wt-PFS ($\beta \approx 3.5$, $K_4/K_2 \approx 0.005$), while the absolute K_2 and K_3 values are the same as those of the P_{RM}wt-PFS. To sum up, we find that a higher rise-time system has higher β and K_i ($i = 2$–4), whereas a lower rise-time system has lower ones. Of course, the rise-time depends on various parameters. However, we especially investigate the dependence of a rise-time on β and K_i for a representative example.

Figure 4(b) shows the rise-time as a function of β and K_3 for the P_{RM}wt-PFS. We find that the PFS with a larger β value has a smaller rise time. It can be interpreted as follows. If β is increased, the feedback activation enhances. This enhancement leads to an increase in the number of the transcriptional products for a given value of x. Hence, many of the products will provide the fast CI accumulation, and in turn, CI will induce further transcription again. As a result, the large feedback activation decreases the rise-time. Next, we consider the K_3 dependency. The increase of K_3 reduces rise-time under the condition that gene expression is fully induced ($X_{max} > 30{,}000$). If K_3 increases, the

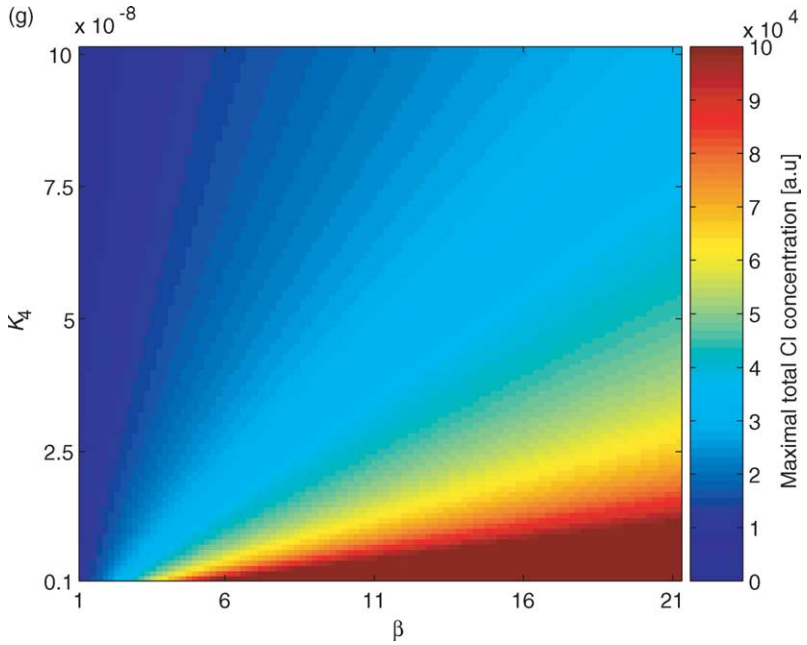

Figure 4. Simulated dynamical behaviors of the positive feedback systems. (a) Simulated gene expression dynamics. Shown is normalized total protein concentration over time. Experiments (points), and the mathematical model using the quantified parameters (continuous line). Blue, the NFS; red, the P_{RM}wt-PFS; green, the P_{RM}L1L1R3-PFS; orange, the P_{RM}R3R2R3-PFS. (b)–(g) The map of rise-time and maximum level of total CI concentration for the P_{RM}wt-PFS. Shown in (b), (d) and (f) are the contour-like maps of rise-time as a function of (β, K_3), (β, K_2) and (β, K_4), respectively. (c), (e) and (g) Maximal GFP concentration as a function of (β, K_3), (β, K_2) and (β, K_4), respectively.

formation of the CI–operator complex becomes frequent. The frequent CI binding increases the chance of transcription per unit time. So, the frequent transcription yields the faster CI accumulation. In turn, the fast accumulation will induce the rapid activation of P_{RM} promoter. As a result, the kinetics of the gene expression become faster, and the rise-time becomes smaller.

It has been already noted that the maximal levels of fluorescence are different among the PFSs. Figure 4(c) presents the total CI-GFP(AAV) concentration as a function of β and K_3. As shown in Figure 4(c), the maximal activator concentration significantly depends on β but not K_3. This result can be interpreted as follows. If x is near the maximal value, we can approximate the production term as $f(x, I) \cong \alpha(I)\beta$ because both $K_3 \gg K_4$ and $K_1K_2K_3x^4 \gg 1$ are satisfied near the steady state. From simple mathematics, we obtain $\alpha(I)\beta/\gamma$ as the approximate maximal total CI concentration. These results suggest that the change of β causes the observed changes of the maximal fluorescence in the variant P_{RM} PFSs. In the P_{RM}L1L1R3-PFS, $\beta \approx 21$ is larger than that of the P_{RM}wt-PFS. Whereas in the P_{RM}R3R2R3-PFS, $\beta \approx 3.5$ is substantially smaller than that of the P_{RM}wt-PFS. The same results hold for the rise-time as a function of β and K_2 (Figure 4(d) and (e)). However, the rise-time is decreased as K_4 becomes larger (Figure 4(f)). This is because K_4 represents repression by the OR3 occupation, so the increase of K_4 leads to the strong negative feedback. Gene expression with the stronger negative feedback is faster than that with the weaker one because the stronger one shuts off its own production to reach the required steady-state concentration[7] (Figure 4(g)). As a result, the rise-time becomes smaller.

It is plausible that the other parameters also affect the rise-time. For example, the model suggests that the increase of the degradation rate of protein γ

Table 1. The variables and the parameters used in the models

	Nomenclature	Wild-type	L1L1R3	R3R2R3
α_{max}	The maximal promoter activity	68±4.7	68±4.7	74±2.0
K_1 ($\times 10^{-4}$)	The dimerization constant	1.0±0.3	1.0±0.4	1.0±0.2
K_2 [$\times 10^{-6}$)	CI dimer-O_0 affinity	1.2±0.4	1.8±0.7	1.1±0.1
K_3 ($\times 10^{-6}$)	CI dimer-O_1 affinity	6.7±2.2	7.1±2.8	6.7±0.5
K_4 ($\times 10^{-8}$)	CI dimer-O_2 affinity	4.1±2.0	4.1±0.8	0.55±0.057
β	The rate of feedback activation	18±3.7	21±3.6	3.5±0.2
γ	The degradation rate	0.014	0.014	0.014
m	The plasmid copy number	10	10	10
s_I ($\times 10^{-4}$)	The leakiness of *lac* regulation	0.25	0.25	0.25
K_I ($\times 10^{-4}$)	The repression factor of *lac* regulation	6.8	6.8	6.8

shifts the rise-time toward the smaller value (data not shown).

Although γ is considered as the constant value, γ can also affect the speed of gene expression (data not shown). We also need to note the difference of the time-evolution at the later time between experiment and model. This discrepancy would be caused by the normalization. The maximal value of gene expression is defined as the CI-GFP(AAV) at the end of this phase, 600 min. However, as the system does not reach the steady state at that time, the experimental maximal values may be underestimated.

Reconstruction of switching behaviors from experimental dynamics

Second, we address the question (II). This exploration is important to understand the hysteretic gene switch.

In this model, the feedback activation and protein multimerization yield non-linearities. These non-linearities lead to a multistable regime in the steady state. The transition from graded (one stable fixed point) to hysteresis (two stable fixed points separated by one unstable fixed point) occurs when equation (3) admits precisely three solutions: this signifies the onset of a saddle-node bifurcation. The behavior of the hysteretic gene network can be described by using equation (3). To analyze the geometric structure of the model, the nullclines of equation (3) are determined as follows.[34] First, $dx/dt=0$ is set to 0, from which follows:

$$\gamma x = \alpha(I)\frac{1 + K_1K_2x^2 + \beta K_1K_2K_3x^4}{1 + K_1K_2x^2 + K_1K_2K_3x^4 + K_1K_2K_3K_4x^6}. \quad (9)$$

equation (9) has fixed points. These fixed points can be found graphically by plotting the left and the right-hand sides of equation (9) and by seeking for the intersections. Figure 5(a) shows that there are one or three intersections, depending on the value of α. Other parameters in the model equations are fixed at the values of the P_{RM}wt-PFS. Assume α is an intermediate value α_m for which there are three intersection x_1, x_2, and x_3 ($x_1<x_2<x_3$) (Figure 5(a), red). As α is decreased from α_m, the two intersections x_2 and x_3 approach each other and eventually coalesce in a saddle-node bifurcation when the line intersects the curve tangentially. If α is decreased further, there is one intersection, x_1, and therefore no additional solutions apart from $x=x_1$ (Figure 5(a), green). On the other hand, as α is increased from α_m, the two intersections x_1 and x_2 approach each other and eventually disappear. The gene expression develops to the sole intersection $x=x_3$ (Figure 5(a), blue). We also find the decrease of $f(x,I)$ around larger values of x. This decline is resulted from the x^6 term. The repression by the OR3 occupation becomes significant as x increases.

In the region with the three intersections, the top and bottom intersections are stable, so that protein concentrations near these values will remain. At the middle point $x=x_2$, the activator degradation and production are equal. However, if x decreases slightly, the resulting positive feedback expression is weaker and x drops to x_1. If x increases slightly, the activator production increases dramatically and x increases to the new fixed point x_3. The middle point is unstable so that tiny fluctuations will drive the protein concentration toward one of the stable states. Hence, within this region, the system will have two experimentally accessible states and thus is multistable. In summary, the fate of the system is determined by the initial state x_0. $x=x_3$ is achieved for $x_0>x_2$. $x=x_1$ is achieved for $x_0<x_2$.

On the other hand, if equation (9) has only one intersection over $0<\alpha<70$ in which corresponds to 0 mM<[IPTG]<1 mM, the model equation produces a graded switch. The sole stable fixed point determines the final state of the system.

Figure 5(a) also reveals an important feature of the system. Hysteresis exclusively occurs if there are one unstable and two stable fixed points. This result is only the case if the curve intersects the line three times. The reason to have three intersections comes from the inflected shape of a curve from a low to a high state. The shape of this curve is determined by the weight of binding activities, x^2, x^4, x^6 and the parameters β and K_i, as described by the term $f(x,I)$. We define that hysteresis occurs if cells exhibit bistable gene expression. The model equations predict that hysteresis occurs between 0.01 mM and 0.018 mM IPTG at the experimental parameter condition (Figure 5(b)). Furthermore, the model equations in which the parameters are fixed at the value of the P_{RM}L1L1R3-PFS also show hysteresis (Figure 5(c)). The parameter region where the hysteretic response appears is included in such a region observed in the experiment. However, the model in which the parameters are fixed at the value of the P_{RM}R3R2R3-PFS switches gene expression in the graded manner the as same as in the experimental result (Figure 5(d)). This is because the model has only a mono-stable fixed point over α (Figure 5(e)). Therefore, the switching behavior is graded, and its gene expression always develops toward a mono-stable point. These simulated results qualitatively agree with the observation on the experiments. However, the parameter region where hysteresis appears is narrower than the experimental results. We will discuss the expansion of the experimental hysteretic region in the Discussion.

The rate of the feedback activation transits switching modes

Although our mathematical model reproduces the experimental results, it remains unknown what the condition is necessary for observing hysteresis, and what molecular mechanism critically determines the transition of switching modes. We answer this problem by using the phase diagram. The phase diagram is useful to know the transition

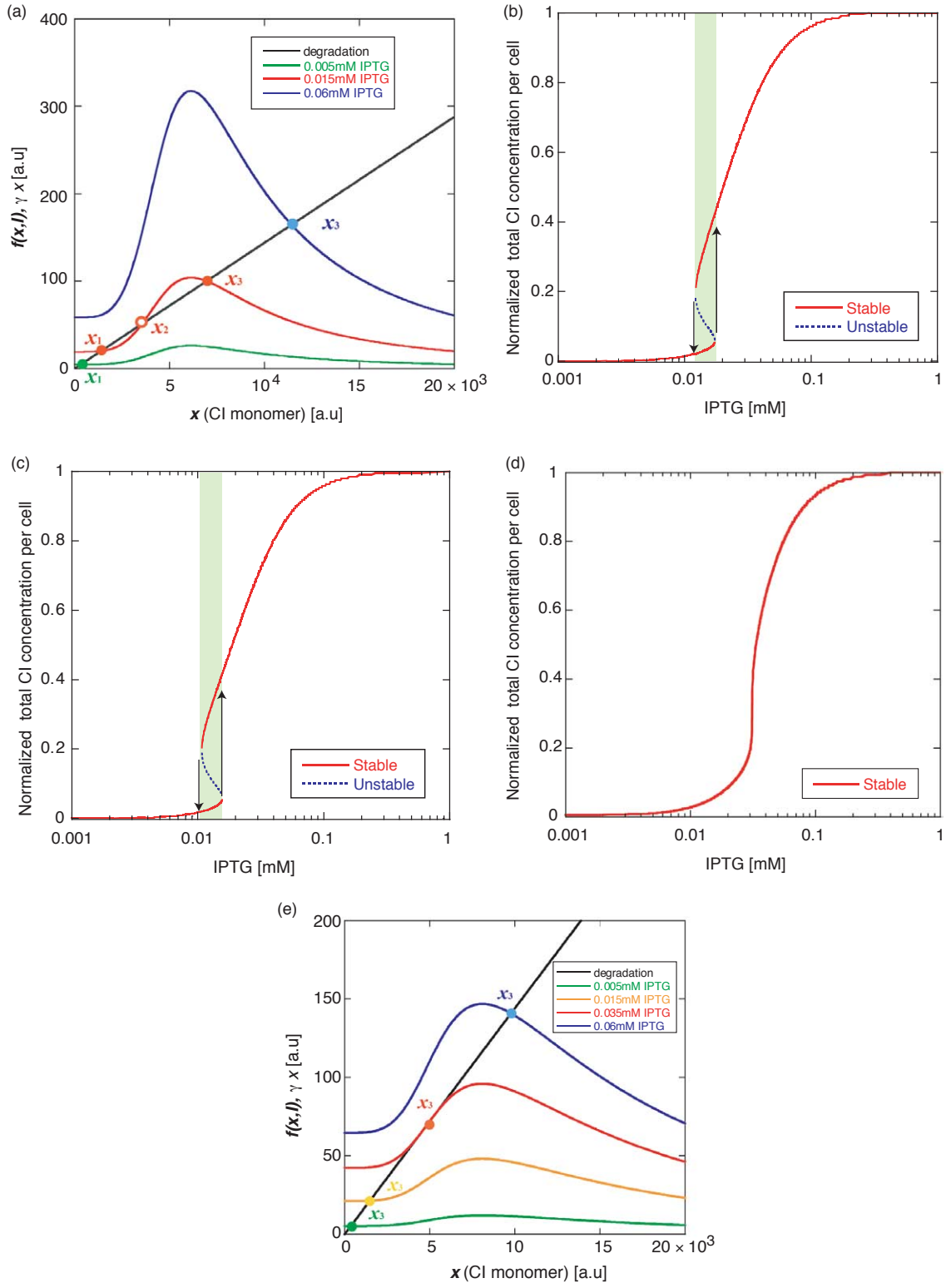

Figure 5. Hysteretic and graded responses reconstructed from the experimental dynamics. Graphical plot of the left and right-hand side of equation (9). For a given α value (which represents the promoter activity and corresponds to the IPTG concentration), the fate of the system is determined by x_0. For $x_0 > x_2$, the final state is $x = x_3$. For $x_0 < x_2$, the resulting final state is $x = x_1$ ($x_1 < x_2 < x_3$). (a) Nullclines of the model of the P_{RM}wt-PFS. Green line, for small α (corresponding to low IPTG concentration and representing low promoter activity), the stable fixed point is only one point (green, filled circle $x = x_1$). Red line, for intermediate α (corresponding to intermediate IPTG concentration and representing intermediate promoter activity α_m), there are three fixed points; filled circle $x = x_1$, open circle $x = x_2$ and filled circle $x = x_3$. The two points are stable (x_1, x_3), but one is unstable (x_2). Blue line, for very large α (increasing IPTG concentration), the two fixed points x_1 and x_2 converge and disappear. The x_3 (blue, Filled circle) is the final state of the system. (b)–(d) Hysteresis in gene expression of positive feedback systems. The mean GFP expression of (b) the model of the P_{RM}wt-PFS

points of switching manners as a function of the parameter.[14]

Figure 6(a) shows the phase diagram for the properties of gene expression of the model in which the other parameters are fixed at the value of the P_{RM}wt-PFS as a function of α and K_3. This Figure shows that gene expression of this model always takes place hysterically. On the contrary, the α-K_3 phase diagram of the model in which the other parameters have the value of the P_{RM}R3R2R3-PFS always shows the graded response (data not shown). As well as K_3, the change of both K_2 and K_4 do not transit the switching behavior (Figure 6(b) and (c)). These results suggest that the affinity between the operator and the activator does not cause the transition of switching behavior.

Next, we examine whether β changes the switching behaviors or not. The α-β phase diagram of the model of P_{RM}wt-PFS shows that the cells exhibit hysteresis around $\beta \approx 18$ (Figure 6(d), dotted line). While β is decreased from the critical point $\beta_c^{wt} \approx 6.2$, the cell also switches gene in a graded fashion, with the expression levels of cells moving continuously between low and high values (Figure 6(d)). As similar, the α-β phase diagram of the model of the P_{RM}R3R2R3-PFS shows that the switching behavior moves from the hysteretic manner to the graded one on reaching a critical value of β, $\beta_c^{R3R2R3} = 3.6$ (Figure 6(e)). The β value of the P_{RM}R3R2R3-PFS is below the critical point β_c^{R3R2R3} (Figure 6(e), dotted line). These results suggest that the experimentally observed change is a shift over the critical point of a α–β phase diagram.

Finally, we consider the reason why the P_{RM}-R3R2R3-PFS has the lower β value as observed in the experiment. We propose the following mechanism as a probable one. Because the highest affinity operator is OR2 in the P_{RM}R3R2R3-PFS, a first CI dimer binds to OR2. But whether a second CI dimer binds to the upstream OR3 or the downstream one with an equal probability. If a second CI dimer binds to the upstream OR3, it functions as the transcriptional activator. On the contrary, if a second CI dimer binds to the downstream OR3, it functions as the transcriptional repressor because the binding competition with RNA polymerase occurs. Such transcriptional repression decreases the effective feedback activation. Such a decrease of the feedback activation causes the transition from a hysteretic to a graded response.

Discussion

This study has demonstrated experimentally and theoretically that the P_{RM} PFS slows down the dynamics of the genetic networks. It is remarkable that the mathematical model predicts that the two mechanisms change the rise-time. One is the rate of the feedback activation and the other is the affinity of the operator–CI dimer interaction. For example, the former decreases the rise-time by the enhancement of the transcription but the latter increases the rise-time by reducing the frequency of the operator–CI complex formation. In addition, we find that cells with the PFS exhibit both the hysteretic and the graded response. The transition of switching behaviors is controlled by the rate of the feedback activation. In this section, we discuss about (1) the biological function of the response delay, (2) the relation between response delay and hysteresis and (3) the origin of the differences between the experimental results and the theoretical calculations.

Biological function of response delay

The important question is whether a response delay induced by the effect of positive feedback is used to perform a certain function in a transcriptional regulatory network. We take the lytic-lysogenic decision of the bacteriophage lambda as a representative example. The CI and Cro regulators define the lysogenic and lytic states, respectively. After an infection, host bacterium almost goes into a lytic state by Cro. This differentiation is made that is dependent upon environmental signals and the number of infecting phages. But if the lysogenic state is chosen, the stable lysogenic prophage is maintained by the P_{RM}-*cI* PFS. Cro is produced from the P_R promoter without regulation, whereas CI is synthesized from the P_{RM} promoter with positive feedback. According to our results, it is expected that the initial rise of Cro production is typically faster than that of CI if the degradation rates of two regulators are identical. Moreover, the rise-time of the P_{RM}wt-PFS is about 120 min. It is larger than the time required for a decision of cell fates, which is 20–30 min.[35] The establishment of the lysogenic state is much later than the period of judgment. Thus, the response delay allows cells to carefully decide their own fate and to turn the lytic state exclusively.

A similar mechanism has been proposed in the flagella synthesis system.[36] The flagella synthesis system also has the positive feedback system composed of the master regulator *fliA*. This PFS acts to prolong the expression of FliA after signal deactivation, and thus to protect flagella production from transient loss of input signal.

Relation between response delay and hysteresis

The second important question is the question (III); what kind of inevitable relation exists or not

(c) the model of the P_{RM}L1L1R3-PFS and (d) the model of the P_{RM}R3R2R3-PFS *versus* the IPTG concentration. Red, low → high (going up); blue, high → low (coming down). The mathematical model reproduces the switching behaviors of the positive feedback systems. (e) Nullclines of the model of the P_{RM}R3R2R3-PFS. Independent of α, the intersection occurred at one point. It means the P_{RM}R3R2R3-PFS does not have multi-stability.

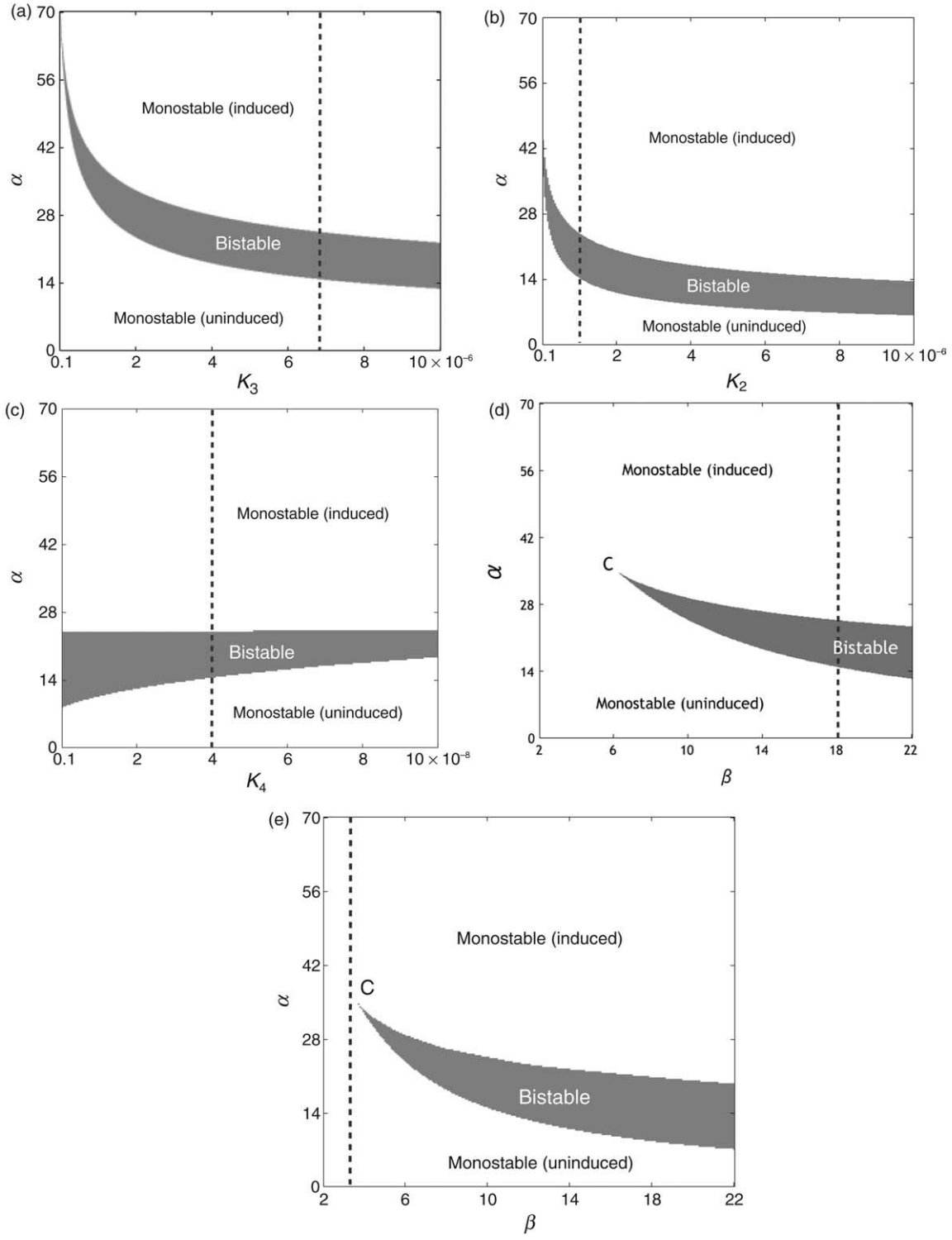

Figure 6. Phase diagram of switching behaviors. The phase diagram of hysteretic and graded responses. It is possible to move from an uninduced state to an induced state either hysteretically (gray region) or in a graded manner (white region). (a) A α-K_3 phase diagram for the model of the P_{RM}wt-PFS: the vertical line indicates α, which corresponds to the IPTG concentrations and also represents the promoter activity. The horizontal line indicates K_3, which represents the affinity of OR2-CI dimer. The dotted line represents the experimental P_{RM}wt-PFS. The region of hysteresis is robust to K_3. (b) A α-K_2 phase diagram for the model of the P_{RM}wt-PFS. (c) A α-K_4 phase diagram for the model of the P_{RM}wt-PFS. The region of hysteresis is also robust to both K_2 and K_4. (d) and (e) α-β phase diagrams; (d) for the model of the P_{RM}wt-PFS; and (e) for the model of the P_{RM}R3R2R3-PFS. The dotted lines in (d) and (e) represent the experimental P_{RM}wt-PFS and the experimental P_{RM}R3R2R3-PFS, respectively. The horizontal line indicates β, which represents the rate of feedback activation. The region of hysteresis grows smaller as β is decreased, eventually reaching a critical point (C) at the rate of feedback activation $\beta_c^{wt} = 6.2$ and $\beta_c^{R3R2R3} = 3.6$, respectively. A graded gene switch is predicted to occur beyond this cusp.

between the response delay and hysteresis? In fact, there is no inevitable relation between the response delay and hysteresis. Cooperativity is not necessary for the PFS to generate the response delay. Even if there is no cooperativity in the PFS (Hill coefficient $n=1$), the response delay arises (Appendix of Kalir, *et al.*[36]). On the other hand, the emergence of bistability (hysteresis) needs cooperativity (Hill coefficient $n \geq 2$). Therefore, the delayed gene expression does not always guarantee the hysteretic gene expression.

For another example, the system with the coherent feed-forward loop has been known to generate the sign-sensitive delay.[37] However, such a system does not exhibit hysteresis because this system only has one stable fixed point. So, the response delay is not also sufficient for hysteresis.

On the other hand, we examine whether the system with the double positive feedback loops, one responds fast and another slower, exhibits the irreversible response the same as hysteresis. However, the significant response delay has not always been observed in such a system.[38] Thus, hysteresis is not also sufficient for the response delay.

From the viewpoint of dynamics, the response time is related to the stability of the equilibrium. If a gene product is initially in an equilibrium state, external or internal perturbations to the steady state will be performed by an exponential decay or rise back to equilibrium. The stability of the fixed point is given by the time constant in the exponential response; high stability corresponds to a fast return to equilibrium, whereas low stability correlates with a slow return. With regard to stability, the central relation is that stability is weakened with activation.[39] So, the response delay is related to the stability of the fixed points, which are weakened by the positive feedback system. However, we need further experimental evidence to prove this consideration at a single cell level.

Comparison between experiments and models

Models based on the experimental dynamics have correctly explained the overall switching behaviors. However, the quantitative differences have been observed between the theoretical calculations and the experimental results. The hysteresis obtained by the experiment is wider than the theoretical prediction. What mechanisms do cause these differences? We propose possible mechanisms by the mathematical analyses.

The experimental hysteresis is observed between 0.0025 mM and 0.05 mM IPTG. However, the model shows the hysteresis at the narrower range near the 0.02 mM IPTG. Concerning the lower IPTG concentration region, we suppose the long-distance interaction between the LacI-*lacO* and the CI-OR2 as a probable mechanism. The long-distance interaction means the spatial interaction of CI dimers with the LacI complex. If the formation of the operator–CI dimer complex inhibits the LacI binding to *lacO*, the relative promoter activity becomes higher at a certain IPTG concentration due to the lower LacI repression. As a result, cells maintain the high state at a lower IPTG concentration. Thereafter, the region which hysteresis occurs will expand.

On the other hand, concerning the higher IPTG concentration region, the observed differences can be reconstructed by several mechanisms: (1) the higher affinity of CI dimer-OR2 binding; (2) non-linear protein degradation.[40] As K_3 is increased, the hysteretic region moves toward the higher IPTG concentration region. However, the discrepancy of dynamics between experiment and model grows larger because the response delay is increased. A more likely mechanism is non-linear protein degradation. If we employ the modified model that involves the non-linear degradation derived from proteolysis of dimer proteins at higher concentrations, instead of the linear degradation, the theoretical hysteretic region expands between 0.02 mM and 0.05 mM IPTG (data not shown). Moreover, the time-evolution agrees with experiments. However, we have not observed the non-linear dependence of the proteolysis of ssrA-tagged proteins yet. The observed expansion of the hysteretic region warrants further exploration.

The present experimental and theoretical study adds the dynamical aspect of the positive feedback system to previously studied motifs such as the feed-forward loop that can act as a sign-sensitive delay element,[37] negative feedback.[7] It would be important to characterize and study additional motifs and their complexes at the dynamical viewpoints in order to understand basic network elements and their functions.

Materials and Methods

Culture and measurements

Single colonies grown on agar plates were inoculated in 1.5 ml LB medium with 50 μg/ml ampicillin and grown overnight at 37 °C with shaking at 200 rpm. The cultures were diluted (1:100(v/v), yielding $A_{600}=0.005$) into fresh minimal medium (solution 1: 2 g of $(NH_4)_2SO_4$, 6 g of Na_2HPO_4, 3 g of KH_2PO_4, 3 g of NaCl, 0.011 g of Na_2SO_4; and solution 2: 0.2 g of $MgCl_2$, 0.01 g of $CaCl_2$, 0.005 g of $FeCl_3 \cdot 7H_2O$ + 2.5 mg thiamine per liter) containing 1 mM glucose as the main carbon source, 0.05%(w/v) Casamino acids as the main nitrogen source, 0.2%(v/v) glycerol and 50 μg/ml ampicillin[41]) in a flat-bottom 96-well plate, at a final volume of 200 μl per well and covered them with 100 μl of mineral oil (Sigma) to avoid evaporation. Cells were grown in a Arvo FX (Perkin Elmer) multiwell fluorimeter at 37 °C and shaken, until $A_{600}=0.1$. Subsequently the dilution 1:10 (v/v) into a fresh medium was done at the same temperature, with various concentrations of IPTG to induce the promoters. After an additional 1.5 h incubation, cultures were assayed with an automatically

repeated protocol of shaking (2 mm double-orbit, normal speed, 30 s), absorbance (A) measurements (600 nm filter, 0.1 s, absorbance through approximately 0.5 cm of fluid), fluorescence readings (ex. 485 nm and em. 535 nm filters, 0.5 s; CW lamp energy 10,000 units), and a delay (120 s). The interval between the repeated measurements was 5 min. The day-to-day reproducibility error of the fluorescence is less than 10%(Figure 2(b) and (c)).

Strains and plasmids

Synthetic genetic networks were constructed using standard molecular cloning techniques as described in basic cloning manuals.[42] All other enzymes were purchased from TOYOBO. All genes, promoters, and transcription terminators were obtained by PCR amplification using Pyrobest polymerase from TaKaRa and primers were from Invitrogen. Genes, promoters and transcription terminators were obtained as follows: $P_{trc\text{-}2}$ promoter was synthesized using two oligonucleotide primers by PCR; P_{RM} promoter and lambda repressor gene, *cI*, were amplified by using isolated prophage genome DNA; *gfp*mut3* and *gfp*(*aav*) including T0T1 terminators from pJBA27 and pJBA112 (gift from S. Molin).[41] The genetic networks were constructed in a middle copy ColE1 plasmid pBR322 because of the ease of genetic manipulation installing networks on the plasmid than in the chromosome.

The plasmid pJMY203 has the P_{RM}wt-PFS where transcription from the P_{RM}-*lacO* promoter drives the expression of the *cI-gfp*(*aav*) fusion gene, P_{RM}-*lacO*::rbsA-*cI-gfp*(*aav*)-T0T1 (Figure 1(a)). When we use the fusion construct, the number of GFP(AAV) and that of CI has a one-to-one correspondence. We inserted *lacO* between P_{RM} and rbsA-*cI-gfp*(*aav*). Gene expression was controlled by IPTG. The background fluorescence was defined as the natural fluorescence from the cells containing pBR322. Another negative control pJMY200, in which encodes P_{RM}-*lacO*::rbsA-*gfp*(*aav*)-T0T1, was also constructed. For constructing pJMY200, *cI* was deleted from pJMY203. The fluorescence of pJMY200 is comparable to the background fluorescence. The low expression level of cells with pJMY200 is due to the absence of CI, because P_{RM} promotes gene expression toward the opposite direction without CI.

However, gene expression of P_{RM}-*loc*O::rbsA-*gfp*(*aav*)-T0T1 is too low to distinguish the background fluorescence. In order to compare the rise-time of the PFS with that of the NFS, we adopted the $P_{trc\text{-}2}$::rbsA-*gfp*(*aav*)-T0T1 construct, in which $P_{trc\text{-}2}$ drives the expression of *gfp*(*aav*) (Figure 1(b)) as the NFS. We constructed the NFS on the plasmid pJMY303. $P_{trc\text{-}2}$ is also controllable with IPTG, because this promoter includes *lacO*. Furthermore, to evaluate the effect of the genetic mutation, we constructed the other plasmids pJMY213 and pJMY233 by introducing several point mutations into P_{RM} in pJMY203. pJMY213 has the promoter, P_{RM}L1L1R3. Conversely, pJMY233 has the promoter, P_{RM}R3R2R3.

The plasmid was introduced into *E. coli* JM109 (genotype: *e14-(McrA-) recA1 endA1 gyrA96 thi-1 hsdR17*(rK-mK+) *supE44 relA1* D(*lac-proAB*) (F′ *traD36 proAB lacI*qZDM15)). At a given IPTG concentration, the maximal expression level of cells with the control pJMY303 is about tenfold of those with pJMY203. The maximal expression levels of cells with pJMY213 and pJMY233 are 1.1-fold and 0.7-fold of those with pJMY203, respectively.

Hysteresis measurements

A single colony grown on agar plates was inoculated in 1.5 ml of LB medium with ampicillin at 37 °C. Cultures containing the PFS were initially grown at 1 mM IPTG with shaking at 200 rpm to confirm a high monostable steady state. The cultures were diluted 1:100(v/v) into a fresh minimal medium either containing or lacking 1 mM IPTG and grown until $A_{600}=0.1$. Cells were suspended and washed in a medium without IPTG. The dilution 1:100 (v/v) into fresh medium with the prescribed concentration of IPTG was done and the cultures were grown for six to seven generations. Fluorescence was measured in cell density $A_{600}=0.1$ using both Arvo FX and a fluorescence spectrophotometer FL-2500 (HITACHI). We measured GFP fluorescence by FL-2500 during logarithmic growth at A_{600} of 0.25. The excitation wavelength was 488 nm, and the emission detection was 514 nm. Cell density was also measured by a spectrophotometer V-5390 (JASCO) at a wavelength of 600 nm.

Mathematical models and parameterization

We provide a detailed description of the derivation of the equations in supporting information. In experiments, we obtained the maximal fluorescence of the total CI-GFP(AAV) from hysteresis measurement at 1 mM IPTG because the gene expression did not saturate during the time-course measurement. In numerical calculations, we defined the maximal total CI concentration X_{max} as $X(t=1000\ \text{min})$. We normalized the kinetics of gene expression by the maximal fluorescence.

For the parameter estimation, we performed by random "best-fit" parameter search on a subset of the parameters (but fixed $\gamma=0.014$). In choosing parameters, we imposed on the parameters as the conditions $K_3>K_2$, $K_4<K_2$, $\beta>1$. This step involved simulating the time-evolution of gene expression. The quality of the model in describing the data is given by the mean error for each PFS:

$$E_j=\frac{1}{T}\sum_{i=1}^{T}\frac{|X_{ij}^{\text{experiment}}-X_{ij}^{\text{theory}}|}{X_{ij}^{\text{experiment}}}, \tag{10}$$

where $X_{ij}^{\text{experiment}}$ (or X_{ij}^{theory}) denotes the experimental (or theoretical) total CI-GFP(AAV) fluorescence per cell at time $t=t_i$ and the PFS j, respectively. We set $E^{\text{Threshold}}=0.02$ for the threshold of each E-value. We found out the parameter sets whose E-values are below the threshold. The mathematical calculation was performed with Matlab 7.0.4.

Acknowledgements

We thank K. Saeki, M. Inaki, E. Takasu H. Iwasaki and T. Kando for their kind experimental advice; and also U. Alon, H.R. Ueda, S. Kuroda, Q. Ouyang, T. Shibata, K. Fujimoto, M. Matsuo, A. Awazu and Y. Murayama for useful discussions. Y.T.M. thanks the Research Fellowships for Young Scientists from the Japan Society for the Promotion of Science 17-12029.

Supplementary Data

Supplementary data associated with this article can be found, in the online version, at doi:10.1016/j.jmb.2006.03.064

References

1. Shen-Orr, S. S., Milo, R., Mangan, S. & Alon, U. (2002). Network motifs in the transcriptional regulation network of *Escherichia coli*. *Nature Genet.* **31**, 64–68.
2. Milo, R., Shen-Orr, S. S., Itzkovitz, S., Kashtan, N., Chklovskii, D. & Alon, U. (2002). Network motifs: simple building blocks of complex networks. *Science*, **298**, 824–827.
3. Becskei, A. & Serrano, L. (2000). Engineering stability in gene networks by autoregulation. *Nature*, **405**, 590–593.
4. Becskei, A., Seraphin, B. & Serrano, L. (2001). Positive feedback in eukaryotic gene networks: cell differentiation by graded to binary response conversion. *EMBO J.* **20**, 2528–2535.
5. Ferrell, J. E. (2002). Self-perpetuating states in signal transduction: positive feedback, double-negative feedback and bistability. *Curr. Opin. Cell Biol.* **14**, 140–148.
6. Austin, D. W., Allen, M. S., McCollum, J. M., Dar, R. D., Wilgus, J. R., Sayler, G. S. *et al*. (2006). Gene network shaping of inherent noise spectra. *Nature*, **439**, 608–611.
7. Rosenfeld, N., Elowitz, M. B. & Alon, U. (2002). Negative autoregulation speeds the response times of transcription networks. *J. Mol. Biol.* **323**, 785–793.
8. Gardner, T. S., Canter, C. R. & Collins, J. J. (2000). Construction of a genetic toggle switch in *Escherichia coli*. *Nature*, **403**, 339–342.
9. Kramer, B. P., Viretta, a. U., Baba, M. D-E., Aubel, D., Weber, W. & Fussenegger, M. (2004). An engineered epigenetic transgene switch in mammalian cells. *Nature Biotechnol.* **22**, 867–870.
10. Johnston, R. J., Jr, Chang, S., Etchberger, J. F., Ortiz, C. O. & Hobert, O. (2005). MicroRNAs acting in a double-negative feedback loop to control a neuronal cell fate decision. *Proc. Natl Acad. Sci. USA*, **102**, 12449–12454.
11. Angeli, D., Ferrell, J. E. & Sontag, E. D. (2004). Detection of multistability, bifurcations,and hysteresis in a large class of biological positive-feedback systems. *Proc. Natl Acad. Sci. USA*, **101**, 1822–1827.
12. Isaacs, J., Hasty, J., Cantor, C. R. & Collins, J. J. (2003). Prediction and measurement of an autoregulatory genetic module. *Proc. Natl Acad. Sci. USA*, **100**, 7714–7719.
13. Ptashne, M. (1992). *Genetic Switch: Phage Lambda and Higher Organisms*, Blackwell Science, Cambridge.
14. Ozbudak, E. M., Thattai, M., Lim, H. N., Shraiman, B. I. & Oudenaarden, A. (2004). Multistability in the lactose utilization network of *Escherichia coli*. *Nature*, **427**, 737–740.
15. Siegele, D. E. & Hu, J. C. (1997). Gene expression from plasmids containing the araBAD promoter at subsaturating inducer concentrations represents mixed populations. *Proc. Natl Acad. Sci. USA*, **94**, 8168–8172.
16. Acar, M., Becskei, A. & Oudenaarden, A. (2005). Enhancement of cellular memory by reducing stochastic transitions. *Nature*, **435**, 228–232.
17. Ferrell, J. E. & Machleder, E. M. (1998). The biochemical basis of an all-or-none cell fate switch in *Xenopus* oocytes. *Science*, **280**, 895–898.
18. Xiong, W. & Ferrell, J. E. (2003). A positive-feedback-based bistable "memory module" that governs a cell fate decision. *Nature*, **426**, 460–464.
19. Bagowski, C. P. & Ferrell, J. E. (2001). Bistability in the JNK cascade. *Curr. Biol.* **11**, 1176–1182.
20. Sha, W., Moore, J., Chen, K., Lassaletta, A. D., Yi, C. S. & Tyson, J. J. (2003). Hysteresis drives cell-cycle transitions in *Xenopus laevis* egg extracts. *Proc. Natl Acad. Sci. USA*, **100**, 975–980.
21. Pomerening, J. R., Sontag, E. D. & Ferrell, J. E. (2003). Building a cell cycle oscillator: hysteresis and bistability in the activation of Cdc2. *Nature Cell. Biol.* **5**, 346–351.
22. Savageau, M. A. (1974). Comparison of classical and autogenous systems of regulation in inducible operons. *Nature*, **252**, 546–549.
23. Sprinzak, D. & Elowitz, M. B. (2005). Reconstruction of genetic circuits. *Nature*, **438**, 443–448.
24. Ackers, G. K., Johnson, A. D. & Shea, M. A. (1982). Quantitative model for gene regulation by lambda phage repressor. *Proc. Natl Acad. Sci. USA*, **79**, 1129–1133.
25. Rosenfeld, N., Young, J. W., Alon, U., Swain, P. S. & Elowitz, M. B. (2005). Gene regulation at the single-cell level. *Science*, **307**, 1962–1965.
26. Atsumi, S. & Little, J. W. (2004). Regulatory circuit design and evolution using phage lambda. *Genes Dev.* **18**, 2086–2094.
27. Sarai, A. & Takeda, Y. (1989). Lambda repressor recognizes the approximately 2-fold symmetric half-operator sequences asymmetrically. *Proc. Natl Acad. Sci. USA*, **86**, 6513–6517.
28. Little, J. W., Shepley, D. P. & Wert, D. (1999). Robustness of a gene regulatory circuit. *EMBO.J.* **18**, 4299–4307.
29. Khlebnikov, A. & Keasling, J. D. (2002). Effect of *lacY* expression on homogeneity of induction from the P_{tac} and P_{trc} promoters by natural and synthetic inducers. *Biotechnol. Prog.* **18**, 672–674.
30. Aurell, E., Brown, S., Johanson, J. & Sneppen, K. (2002). Stability puzzles in phage λ. *Phys. Rev. E*, **65**, 051914.
31. Shea, M. A. & Ackers, G. K. (1985). The O_R control system of bacteriophage lambda: a physical–chemical model for gene regulation. *J. Mol. Biol.* **181**, 211–230.
32. Setty, Y., Mayo, A. E., Surette, M. G. & Alon, U. (2003). Detailed map of a *cis*-regulatory input function. *Proc. Natl Acad. Sci. USA*, **100**, 7702–7707.
33. Pray, T. R., Burz, D. S. & Ackers, G. K. (1998). Cooperative non-specific DNA binding by octamerizing λcI repressors: a site-specific thermodynamic analysis. *J. Mol. Biol.* **282**, 947–958.
34. Kramer, B. P. & Fussenegger, M. (2005). Hysteresis in a synthetic mammalian gene network. *Proc. Natl Acad. Sci. USA*, **102**, 1848–1852.
35. Kobiler, O., Rokney, A., Friedman, N., Court, D. L., Stavans, J. & Oppenheim, A. B. (2005). Quantitative kinetic analysis of the bacteriophage λ genetic network. *Proc. Natl Acad. Sci. USA*, **102**, 4470–4475.
36. Kalir, S., Mangan, S., & Alon, U. (2005). A coherent feed-forward loop with a SUM input function prolongs flagella expression in *Escherichia coli*. *Molecular Systems Biology*, msb4100010-E1-msb 4100010-E6. Publisher, Town.

37. Mangan, S., Zaslaver, A. & Alon, U. (2003). The coherent feedforward loop serves as a sign-sensitive delay element in transcriptional networks. *J. Mol. Biol.* **334**, 197–204.
38. Brandman, O., Ferrell, J. E., Jr, Li, R. & Meyer, T. (2005). Interlinked fast and slow positive feedback loops drive reliable cell decisions. *Science*, **310**, 496–498.
39. Hasty, J., McMillen, D., Isaacs, F. & Collins, J. J. (2001). Computational studies of gene regulatory networks: *in numero* molecular biology. *Nature Rev. Genet.* **2**, 268–279.
40. Buchler, N. E., Gerland, U. & Hwa, T. (2005). Nonlinear protein degradation and the function of genetic circuits. *Proc. Natl Acad. Sci. USA*, **102**, 9559–9564.
41. Andersen, J. B., Sternberg, C., Poulsen, L. K., Björn, S. P., Givskov, M. & Molin, S. (1998). New unstable variants of green fluorescent protein for studies of transient gene expression in bacteria. *Appl. Environ. Microbiol.* **64**, 2240–2246.
42. Sambrook, J. & Russell, D. W. (2001). *Molecular Cloning: A Laboratory Manual* (3rd edit.) *3rd*, Cold Spring Harbor Laboratory Press, Plainview, NY.

Edited by R. Ebright

(Received 29 March 2006; accepted 29 March 2006)
Available online 27 April 2006